



HAL
open science

Global statistical maps of extreme-event magnetic observatory 1 min first differences in horizontal intensity

Jeffrey J. Love, Pierdavide Coïsson, Antti Pulkkinen

► To cite this version:

Jeffrey J. Love, Pierdavide Coïsson, Antti Pulkkinen. Global statistical maps of extreme-event magnetic observatory 1 min first differences in horizontal intensity. *Geophysical Research Letters*, 2016, 43, pp.4126-4135. 10.1002/2016GL068664 . insu-03748797

HAL Id: insu-03748797

<https://insu.hal.science/insu-03748797>

Submitted on 10 Aug 2022

HAL is a multi-disciplinary open access archive for the deposit and dissemination of scientific research documents, whether they are published or not. The documents may come from teaching and research institutions in France or abroad, or from public or private research centers.

L'archive ouverte pluridisciplinaire **HAL**, est destinée au dépôt et à la diffusion de documents scientifiques de niveau recherche, publiés ou non, émanant des établissements d'enseignement et de recherche français ou étrangers, des laboratoires publics ou privés.



Distributed under a Creative Commons Attribution - NonCommercial - ShareAlike 4.0 International License



RESEARCH LETTER

10.1002/2016GL068664

Key Points:

- We construct latitude-dependent maps of geomagnetic activity using time series of ground observatory data
- Results summarize the occurrence probability and magnitude of extreme-event magnetic storms
- This work is motivated by power grid industry needs and national space weather strategic plans

Correspondence to:

J. J. Love,
jlove@usgs.gov

Citation:

Love J. J., P. Coïsson, and A. Pulkkinen (2016), Global statistical maps of extreme-event magnetic observatory 1 min first differences in horizontal intensity, *Geophys. Res. Lett.*, *43*, 4126–4135, doi:10.1002/2016GL068664.

Received 12 MAR 2016

Accepted 5 APR 2016

Accepted article online 11 APR 2016

Published online 10 MAY 2016

©2016. The Authors.

This is an open access article under the terms of the Creative Commons Attribution-NonCommercial-NoDerivs License, which permits use and distribution in any medium, provided the original work is properly cited, the use is non-commercial and no modifications or adaptations are made.

Global statistical maps of extreme-event magnetic observatory 1 min first differences in horizontal intensity

Jeffrey J. Love¹, Pierdavide Coïsson², and Antti Pulkkinen³

¹U.S. Geological Survey Geomagnetism Program, Denver, Colorado, USA, ²Institut de Physique du Globe de Paris, Sorbonne Paris Cité, Université Paris Diderot, Centre National de la Recherche Scientifique, Paris, France, ³NASA Goddard Space Flight Center, Greenbelt, Maryland, USA

Abstract Analysis is made of the long-term statistics of three different measures of ground level, storm time geomagnetic activity: instantaneous 1 min first differences in horizontal intensity ΔB_h , the root-mean-square of 10 consecutive 1 min differences S , and the ramp change R over 10 min. Geomagnetic latitude maps of the cumulative exceedances of these three quantities are constructed, giving the threshold (nT/min) for which activity within a 24 h period can be expected to occur once per year, decade, and century. Specifically, at geomagnetic 55° , we estimate once-per-century ΔB_h , S , and R exceedances and a site-to-site, proportional, 1 standard deviation range [1 σ , lower and upper] to be, respectively, 1000, [690, 1450]; 500, [350, 720]; and 200, [140, 280] nT/min. At 40° , we estimate once-per-century ΔB_h , S , and R exceedances and 1 σ values to be 200, [140, 290]; 100, [70, 140]; and 40, [30, 60] nT/min.

1. Introduction

Magnetic storms are hazardous for modern technological infrastructure [e.g., Cannon *et al.*, 2013]. Of particular concern is the induction of geoelectric fields in the Earth's electrically conducting interior [e.g., Thomson, 2007]. Intense magnetic storms can induce intense geoelectric fields, and these can interfere with the operation of electric power grids [e.g., Boteler, 2003]. The reality of induction hazards was demonstrated during the March 1989 magnetic storm [e.g., Allen *et al.*, 1989], when the Hydro-Québec electric power grid in Canada was caused to collapse [Béland and Small, 2005]. Some scenario analyses suggest that the future occurrence of an extreme-event magnetic storm could cause widespread failure of electric power grid operations, with deleterious economic consequences [Baker *et al.*, 2008]. This possibility has motivated regulatory agencies in the United States to require utility companies to take mitigating measures so as to avoid geomagnetic interference with the operation of bulk electric power systems [Federal Energy Regulatory Commission, 2013, Order No. 779]. In parallel to these developments, national and international strategic planning [e.g., National Science and Technology Council (NSTC), 2015a; Schrijver *et al.*, 2015] is helping to focus research on the natural science of induction hazards and extreme space weather events [e.g., Hapgood, 2011].

For induction hazard assessment projects [e.g., Thomson *et al.*, 2009; Love *et al.*, 2014], geoelectric fields can be estimated [e.g., Pirjola, 1984] by convolving geomagnetic time series through an impedance tensor that is, itself, a function of the Earth's electrical conductivity structure. Geoelectric fields drive uncontrolled, quasi-direct currents in power grids. Qualitatively, it is observed that the amplitude of these currents increases with the intensification of the “ dB/dt ” rate of change of geomagnetic field variation [e.g., Kappenman, 2005, Figure 7; Trichtchenko and Boteler, 2007, Figure 3; Viljanen, 1997, Figure 5]. In this study, we analyze the statistics of global geomagnetic activity as recorded by minute-to-minute first differences in magnetic observatory time series ΔB_h . We use these first differences to characterize the global occurrence probability of rare, but extremely intense, geomagnetic activity events, thus building on previously published work that is either focused on a particular geographic region [e.g., Thomson *et al.*, 2011, Europe, Figure 6] or on specific magnetic storms [Pulkkinen *et al.*, 2012, Figure 4; Ngwira *et al.*, 2013a, Figure 2]. Results inform the development of magnetic storm geoelectric benchmarks needed by the power grid industry [e.g., NSTC, 2015b, Goal 1.1].

2. Observatory Data

Time series of 1 min resolution magnetometer data have been collected at many observatories [e.g., Love, 2008] for many years and at a widely distributed set of sites. Routine collection of 1 min data began at

Table 1. Summary of Observatory Data Used in This Analysis; Geomagnetic Latitudes for 1995

	Name	Mag. Lat Mag. Long.		Data Range	Years Omitted	Present Operating Institute
		(°N)	(°E)			
THL	Thule	87.32	14.38	1985–2013		Technical University of Denmark
RES	Resolute	82.73	305.95	1978–2013	1980, 1991	Geological Survey of Canada
GDH	Godhavn	78.16	33.82	1976–2013	2007–2008	Technical University of Denmark
DRV	Dumont d’Urville	–74.11	230.87	1981–2011		Ecole et Observatoire des Sciences de la Terre
BLC	Baker Lake	72.86	323.39	1979–2012		Geological Survey of Canada
NAQ	Narsarsuaq	69.49	38.58	1982–2013	2009–2010	Technical University of Denmark
BRW	Barrow	69.68	247.44	1975–2013	1975–1978	U.S. Geological Survey
YKC	Yellowknife	68.71	300.63	1978–2013		Geological Survey of Canada
ABK	Abisko	65.98	114.33	1979–2014	1980	Geological Survey of Sweden
CMO	College	65.36	262.77	1978–2012		U.S. Geological Survey
MEA	Meanook	61.29	307.20	1978–2013		Geological Survey of Canada
SIT	Sitka	60.20	281.38	1978–2014		U.S. Geological Survey
ESK	Eskdalemuir	57.52	83.66	1983–2013		British Geological Survey
PAF	Port-aux-Francais	–56.62	133.63	1974–2011		Ecole et Observatoire des Sciences de la Terre
OTT	Ottawa	55.18	355.89	1979–2013		Geological Survey of Canada
NEW	Newport	54.57	305.5	1982–2013		U.S. Geological Survey
HAD	Hartland	53.60	80.16	1983–2013		British Geological Survey
CZT	Crozet	–51.12	114.12	1974–2012		Ecole et Observatoire des Sciences de la Terre
BEL	Belsk	50.06	105.18	1985–2012		Polish Academy of Sciences
CLF	Chambon-la-Forêt	49.56	85.72	1980–2013		Institut de Physique du Globe de Paris
FRD	Fredericksburg	47.95	353.94	1982–2014		U.S. Geological Survey
BOU	Boulder	48.05	321.32	1978–2014		U.S. Geological Survey
AMS	Martin De Vivies	–46.03	144.96	1981–2009		Ecole et Observatoire des Sciences de la Terre
FRN	Fresno	43.24	305.97	1982–2013		U.S. Geological Survey
BSL	Stennis	39.66	340.37	1986–2012		U.S. Geological Survey
TUC	Tucson	39.56	316.77	1982–2014		U.S. Geological Survey
MMB	Memambetsu	35.44	211.77	1985–2013		Japan Meterological Agency
HER	Hermanus	–33.91	84.67	1974–2013	1975	South African National Space Agency
SJG	San Juan	27.92	6.53	1983–2014		U.S. Geological Survey
KAK	Kakioka	27.47	209.23	1976–2013		Japan Meterological Agency
HON	Honolulu	21.59	270.30	1983–2013		U.S. Geological Survey
KNY	Kanoya	22.00	201.21	1985–2013		Japan Meterological Agency
PPT	Pamatai	–15.03	285.47	1986–2012	1991, 1996	Institut de Physique du Globe de Paris
GUA	Guam	5.48	216.09	1983–2014		U.S. Geological Survey

observatories in the 1970s, a significant improvement from 1 h resolution data. Today, many observatories collect 1 s resolution data, but their total time span of 1 s time series is not yet long enough to be even close or comparable to those of the 1 min data, which record multiple magnetic storms of high intensity. Here we analyze horizontal intensity observatory data collected since 1974 from the 34 observatories listed in Table 1; a geomagnetic coordinate map of observatory locations is given in Figure 1; note that over the time span of the data collected for the listed observatories, geomagnetic coordinates change only slightly relative to other variation factors affecting this analysis. The data from each observatory consist of discrete samples that we represent as $B_H(t_i)$, for time stamp values $t_i, t_{i+1}, t_{i+2}, \dots$, where $\tau = t_{i+1} - t_i$ is the 1 min sequence interval. From the listed observatories, there are a total of 567,609,075 individual 1 min “definitive” data values that have had (most) spikes and other artifacts removed. We examine each time series from each observatory for spikes; data for a few years from a few observatories are noisy; these are removed from our analysis (e.g., BRW 1975–1978; PPT 1991, 1996). In some cases, for some years in the middle of a long period of observatory operation, definitive data are not available (e.g., HER 1975; NAQ 2009–2010).

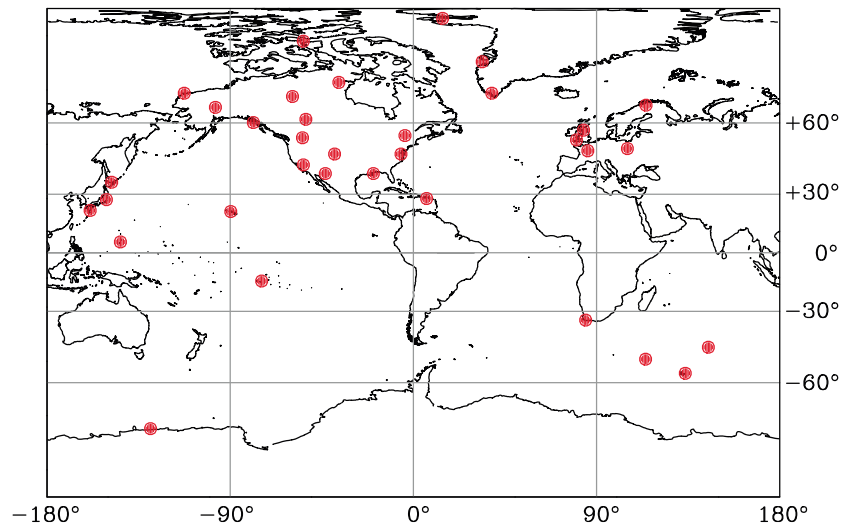


Figure 1. Geomagnetic-coordinate, Miller-projection map of the locations of the observatories for which 1 min resolution data are used in this analysis.

3. Time Series

A magnetic storm amounts to a transient enhancement in geomagnetic disturbance, often commencing suddenly, growing in strength, and then gradually returning to relative quiescence. In detail, however, the time evolution of every storm is different, and some storms exhibit more rapid magnetic variation than others. A simple and standard measure of storm variation consists of absolute value, 1 min, (forward) first differences of the horizontal field component

$$\Delta B_h(t_i) = \frac{1}{\tau} |B_h(t_{i+1}) - B_h(t_i)| \tag{1}$$

[e.g., *Viljanen et al., 2001*], which has units of nT/min. In Figure 2, we show ΔB_h time series, 1983–2013, from several observatories situated across a broad range of geomagnetic latitudes, from College, Alaska (CMO), where ΔB_h activity is relatively high, to San Juan, Puerto Rico (SJG), where ΔB_h activity is relatively low. On this scale, individual magnetic storms correspond to large ΔB_h values; clearly identifiable as local maxima, for example, are the great storms of October and November 2003, which resulted in operational stress for numerous technological systems [e.g., *Balch et al., 2004*], including power grid systems [e.g., *Pulkkinen et al., 2005; Thomson et al., 2005*]. Also seen in Figure 2 is a quasi-periodic 11 year solar cycle modulation in geomagnetic activity.

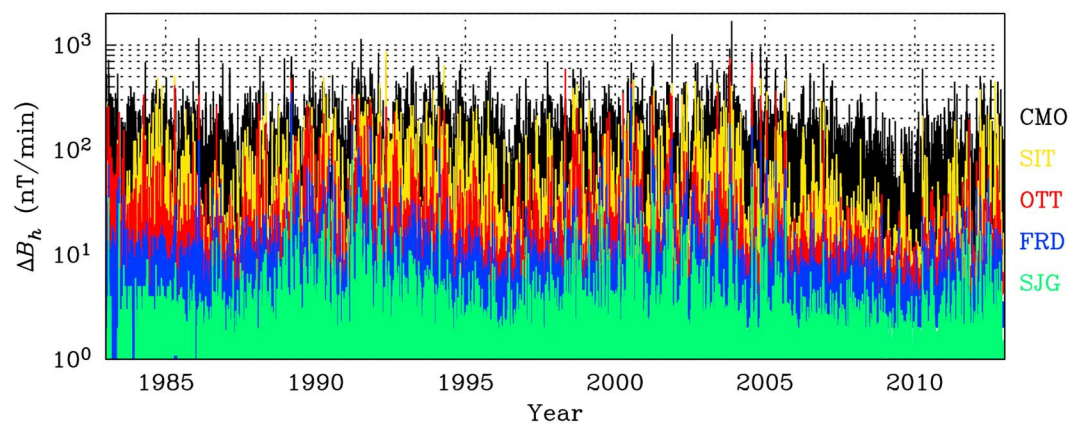


Figure 2. Time series of 1 min ΔB_h for 30 years, from the beginning of 1983 to the end of 2013, from several observatories situated across a broad range of geomagnetic latitudes, from College, Alaska (CMO, 65.36°N), where ΔB_h activity is relatively high, to San Juan, Puerto Rico (SJG, 27.92°N), where ΔB_h activity is relatively low.

4. Statistics for Each Observatory

Acknowledging that every magnetic storm has its own detailed evolution, we consider the statistics of three different measures of magnetic activity: individual, 1 min $\Delta B_h(t_i)$ as given by (1), the 10 min, ramp change $R(t_i)$ given by the absolute value of the 10 min average change, $m(t_i)$, in horizontal intensity

$$R(t_i) = |m(t_i)| = \frac{1}{10 \cdot \tau} \left| \sum_{j=1}^{10} [B_h(t_{i+j}) - B_h(t_{i-1+j})] \right| = \frac{1}{10 \cdot \tau} |B_h(t_{i+10}) - B_h(t_i)|, \quad (2)$$

and the 10 min, root-mean-square $S(t_i)$ of change,

$$S^2(t_i) = \frac{1}{10 \cdot \tau^2} \sum_{j=1}^{10} [\Delta B_h(t_{i+j}) - m(t_i)]^2, \quad (3)$$

where, again, and in each case, τ is the 1 min data sequence interval. Note that, in some respects, R is a 10 min first difference, and so analogous to the 1 min first difference ΔB_h . The 1 min and 10 min timescales of these different measures of magnetic activity fall within the range of timescales (tens of seconds to about an hour) that utility companies have considered in the evaluation of the vulnerability of high-voltage transformers to geomagnetically induced currents (GIC) [e.g., *North American Electric Reliability Corporation (NERC)*, 2014a, 2014b].

Comparison of specific values is worthwhile. First, we note that the moment in time of the largest activity values at a given observatory is not necessarily simultaneous with the largest value at another observatory. So, for example, the largest individual ΔB_h value recorded at the Chambon-la-Forêt, France (CLF), occurred on 24 March 1991 (200 nT/min), while the largest ΔB_h value for Belsk, Poland (BEL), occurred during the so-called Bastille Day storm of 15 July 2000 (214.6 nT/min). The largest S value for CLF occurred on 24 March 1991 (77.7 nT/min), while for BEL it occurred on 31 October 2003 (103.3 nT/min); the largest R values for CLF (37.9 nT/min) and BEL (68.2 nT/min) both occurred on 29 October 2003. Second, among all the data analyzed, the single largest recorded ΔB_h value (3037.5 nT/min) occurred at Narsarsuaq, Greenland (NAQ), on 29 October 2003; the largest recorded S value (601.4 nT/min) also occurred at Barrow, Alaska (BRW), on 22 September 1982; the largest recorded R value (76.0 nT/min) occurred at Godhavn, Greenland (GDH), on 13 July 1982. And, third, the largest ΔB_h value recorded for Ottawa, Ontario (OTT), occurred on 29 October 2003 (758.0 nT/min); this exceeded the maximum value for OTT during the Québec storm on 14 March 1989 (484.5 nT/min).

We subsample the ΔB_h , S , and R activity data from each observatory to reduce autocorrelation that can give inflated measures of statistical significance. We rank the activity data by size, identify the largest value for a given time t_i , keep it for statistical analysis, and exclude from further analysis all other data within a 1 day window $[t_{i+720}, t_{i-720}]$; the process is repeated with the remaining data, and the algorithm terminates when the largest remaining value is below some threshold. We treat each of the remaining data values as discrete statistical events—each for a day with a measured level of maximum ΔB_h , S , and R activity. Obviously, this process of ranking and winnowing reduces considerably the number of data analyzed, but since most substorms have characteristic timescales of an hour or two [e.g., *Borovsky et al.*, 1993], the remaining autocorrelation is tiny. We are left with “declustered” data recording the largest values of ΔB_h , S , and R within 24 h, 1 day durations.

5. Lognormal Models

Drawing upon related and previously published work [e.g., *Pulkkinen et al.*, 2008; *Love et al.*, 2015], we assume that the declustered activity data ΔB_h , S , and R can be modeled by a lognormal distribution that is truncated at the chosen lower size threshold. A random positive variable x is the realization of a lognormal statistical process if its probability density is

$$\lambda(x|v, \epsilon^2) = \frac{1}{x\sqrt{2\pi\epsilon^2}} \exp \left[-\frac{(\ln x - v)^2}{2\epsilon^2} \right], \quad (4)$$

where v and ϵ^2 are model parameters. The occurrence probability for events with size exceeding x is given by the cumulative

$$\Lambda(x|v, \epsilon^2) = \int_x^\infty \lambda(\xi|v, \epsilon^2) d\xi. \quad (5)$$

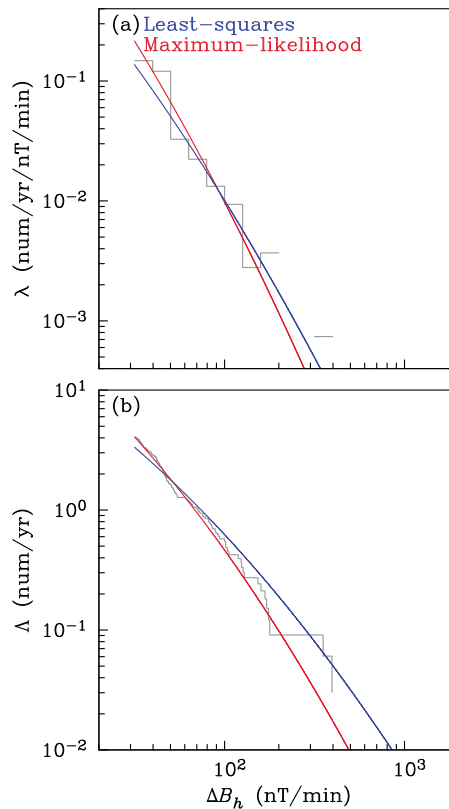


Figure 3. For declustered ΔB_h activity data from Fredericksburg (FRD), 1982–2014, (a) binned rate densities (gray), least squares fit of truncated lognormal model (blue), maximum likelihood fit (red), and (b) the corresponding cumulatives (giving the number of days per year in which activity can be expected to exceed a given threshold).

Taking x to represent the declustered activity data ΔB_h , S , and R , we define a rate function,

$$\rho(x|A, v, \epsilon^2) = A \cdot \lambda(x|v, \epsilon^2), \tag{6}$$

where A is a normalizing amplitude such that,

$$A \int_{\theta}^{\infty} \lambda(\xi|v, \epsilon^2) d\xi = \frac{N(x_j \geq \theta)}{T}, \tag{7}$$

where N is the number of days with data larger than θ , and where T is the total span of the observatory time series. Following *Love et al.* [2015], we obtain model parameters $\{A, v, \epsilon^2\}$ by fitting equation (6) to the x_j data using weighted least squares and maximum likelihood methods.

6. FRD Lognormal Results

In Figure 3a, we show binned rate densities for ΔB_h data from the Fredericksburg, Virginia observatory (FRD), for the years 1982–2014; in Figure 3b, we show corresponding results for rate cumulatives. We choose to fit a decade range of the declustered FRD ΔB_h data: those ΔB_h slightly greater than 31.6 nT/min—corresponding to a bin boundary—up to the largest recorded ΔB_h value of 395.3 nT/min, which was realized on 15 July 2000. There are 134 declustered FRD events such that $\Delta B_h \geq 31.6$ nT/min for the years 1982–2014 (out of a total of 16,438,421 first differences). In Figure 3, we show both weighted least squares and maximum likelihood lognormal fits to the FRD data. Note that the least squares fit is an accurate representation of the data over the full range of the ΔB_h bins, including the most extreme value bin: $\Delta B_h \in [316, 398]$ nT/min; on the other hand, the maximum likelihood fit is an accurate representation of the majority of the ΔB_h data, which are mostly at the smaller event end of the range of ΔB_h . As for statistical significance, a relative χ^2 measure for FRD would be a likely realization of random data, $p = 0.96$. Therefore, we cannot reject the null hypothesis that the data are

lognormal. Similarly, the Kolmogorov-Smirnov D measure would be a moderately likely realization of random data, $p = 0.49$. Again, we cannot reject the lognormal hypothesis.

The model fits to the FRD ΔB_h data can be used to estimate the number of days per year in which activity can be expected to exceed a given threshold (a cumulative exceedance). From a least squares fit, we can estimate that days with ΔB_h greater than 74.2 nT/min occur typically once per year; similarly, days with ΔB_h events greater than 281.9 nT/min and 852.9 nT/min occur typically once per decade and once per century (the latter is 2.2 times greater than the largest recorded value, Bastille Day storm). From a maximum likelihood fit the corresponding results are, respectively, 68.5 nT/min, 198.5 nT/min, and 490.8 nT/min (1.2 times greater than Bastille). Differences between the least squares and maximum likelihood exceedance values give some idea of the uncertainty in their estimation, especially for once-per-century return rate extrapolations.

7. Latitude Map of Activity Exceedance

In Figure 4 and Table 2, we provide, as a function of observatory-location geomagnetic latitude (assumed symmetric under reflection through the geomagnetic equator), estimates of the ΔB_h , S , and R cumulative exceedances for events occurring typically once per year, decade, and century, each for both least squares and maximum likelihood fits; Figures 4a and 4d can be compared with, e.g., Thomson *et al.* [2011, Figure 6] for Europe, with Pulkkinen *et al.* [2012, Figures 4c and 4d] for the 1989 Québec and 2003 Halloween storms, and with Ngwira *et al.* [2013a, Figure 2] for several intense storms. For each activity measure, we fit a simple (and purely phenomenological) function of geomagnetic latitude ϕ consisting of a polynomial, parameterized by $\{\alpha_0, \dots, \alpha_4\}$, plus a term that allows for a kink, parameterized by $\{\beta, \gamma, \delta\}$:

$$p(\phi) = 10^{e(\phi)} \quad (8)$$

where

$$e(\phi) = \beta \cdot \left| \left(\frac{\phi}{90^\circ} \right) - \delta \right|^\gamma + \sum_{k=0}^4 \alpha_k \cdot \left(\frac{\phi}{90^\circ} \right)^k. \quad (9)$$

We fit $e(\phi)$ to the logarithms of the ΔB_h , S , and R exceedances using a least squares algorithm, subject to derivative constraints at the geomagnetic equator and pole:

$$\partial_\phi p(0^\circ) = 0 \text{ and } \partial_\phi p(90^\circ) = 0. \quad (10)$$

The (vertical axis) range in all three of the exceedance quantities is about a factor of 10, with steep change between latitudes 40° and 60°; qualitatively, the latitudinal dependence is seen in other studies [e.g., Thomson *et al.*, 2011], including in the scaling factor used for the North American Electric Reliability Corporation benchmark [NERC, 2014a, Table II-1]. For the once-per-century extrapolation of the ΔB_h , S , and R exceedances, we measure the observatory-to-observatory scatter about the fitted curve, and we plot corresponding to a proportional, 1 standard deviation [1σ , lower and upper] range given by $10^{\pm\sigma} \times p(\phi)$. For least squares results, the ΔB_h 1σ range is $[0.63, 1.58] \times p(\phi)$, while for maximum likelihood results it is $[0.76, 1.32] \times p(\phi)$. Note that the least squares results (left) are generally within the 1σ range obtained for maximum likelihood results (right) and vice versa; and so the two methods yield essentially similar results.

We see in Figure 4 that the kinks (maxima) in the fitted functions for the once-per-century maximum ΔB_h , S , and R exceedance values occur within a 58° to 62° latitude band. Here the once-per-century maximum ΔB_h exceedance is approximately 2000 nT/min, or roughly that found by Thomson *et al.* [2011, Figure 6b] from their extreme-value statistical analysis of ΔB_h data from Europe. The location of the kinks tend toward lower latitudes for rarer exceedances—once-per-decade events are displaced equatorward of once-per-year events, etc. This is consistent with the well-known equatorward shift of the auroral oval that occurs during intense magnetic storms, even though our work with magnetic activity data does not specifically identify the latitudinal extent of the auroral oval. And, indeed, the maximum activity band is equatorward of the usual 70° location of the auroral oval [e.g., Milan, 2007].

More specifically, the largest once-per-century least squares ΔB_h exceedance (3745.2 nT/min) in Figure 4a is from Newport, Washington State (NEW, 54.57°N), while the corresponding maximum likelihood exceedance is not as anomalously large (1442.1 nT/min), both of which are greater than the largest directly measured

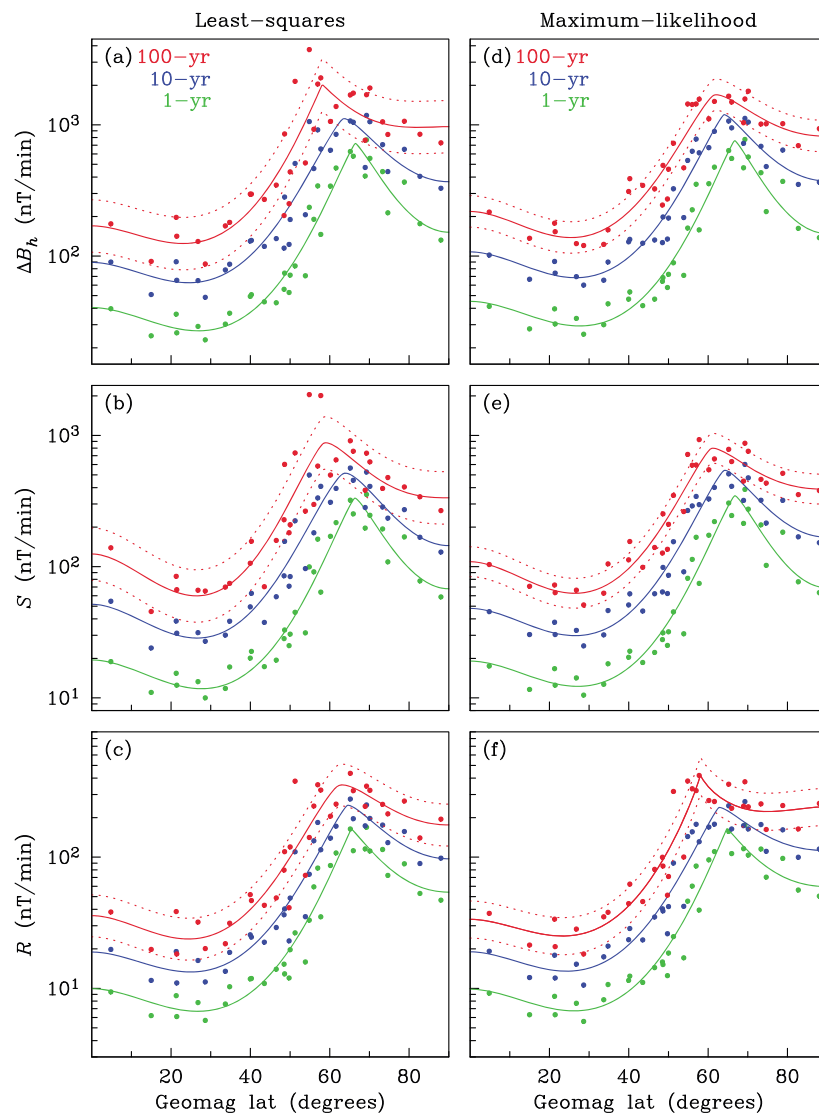


Figure 4. Magnetic latitude maps obtained, respectively, by least squares and maximum likelihood methods, of (a, d) ΔB_h , (b, e) S , and (c, f) R cumulative exceedances, the threshold (nT/min) for which activity within a 24 h period can be expected to occur once per year (green), decade (blue), and century (red). Dots correspond to values taken from lognormal fits to data from individual observatories; dotted lines show 1 standard deviation (1σ lower and upper) range.

value at this observatory (384.7 nT/min, 5 June 1991). There are many possible explanations for this, including the fact that the weighted least squares estimations, obtained by fitting binned data, are not as stable as the maximum likelihood estimations, obtained by fitting unbinned data [e.g., Love *et al.*, 2015, section 8]. The once-per-century least squares NEW (Newport) value is compared to the largest directly measured ΔB_h value from NAQ (69.49°N, 3037.5 nT/min, 29 October 2003). Still, all of these values are smaller than the 5000 nT/min value that Kappenman [2006] has inferred for Lovo, Sweden, as having possibly occurred during the great storm of May 1921 (long before 1 min digital data were available).

The lowest exceedance values occur at latitudes of about 25°, where magnetic activity is affected by currents in the magnetopause and equatorial magnetosphere; here the once-per-century minimum ΔB_h exceedance is approximately 130 nT/min. For comparison, Araki *et al.* [1997] report that the largest sudden commencement impulse ever recorded at Kakioka, Japan (KAK, 27.47°N), is 202 nT, 24 March 1991, but the duration of this impulse was less than a minute (not resolvable in the data used here). Tsurutani and Lakhina [2014] estimate a theoretical upper value for a low-latitude sudden commencement impulse of 234 nT, transpiring over 22 s (again, not resolvable). Closer to the equator, observatories are sparsely distributed; very close to the equator,

Table 2. Latitude Map Model Parameters for Fits Shown in Figure 4^a

Rate (years)	α_0	α_1	α_2	α_3	α_4	β	δ	γ	σ
(a) ΔB_h Least Squares									
100	5.7478	-5.7646	-6.5319	21.2017	-9.8024	-5.5883	0.6457	1.0581	0.1991
10	12.1220	-21.4619	0.3846	22.5153	-8.1969	-17.1209	0.7044	1.4865	0.1506
1	9.3834	-13.1726	-4.2571	17.5725	-5.2180	-11.3653	0.7382	1.2506	0.1193
(b) S Least Squares									
100	16.2437	-34.9659	3.4740	40.0239	-16.9961	-28.2831	0.6495	1.6053	0.1988
10	11.7491	-20.5710	-1.4935	23.7722	-8.5291	-16.5074	0.7117	1.4544	0.1083
1	10.6396	-16.7333	-4.0004	20.5304	-6.2024	-13.9846	0.7370	1.3188	0.1183
(c) R Least Squares									
100	19.1817	-43.5240	13.9852	28.0894	-10.9966	-33.1466	0.6905	1.7048	0.1606
10	9.3851	-15.9285	-2.0824	20.2574	-7.4350	-12.9726	0.7160	1.4065	0.1225
1	7.3817	-10.5987	-4.5023	16.8672	-5.6455	-9.2748	0.7377	1.2229	0.1131
(d) ΔB_h Maximum Likelihood									
100	13.9106	-27.0710	3.3528	27.0222	-10.8833	-21.3030	0.6822	1.5961	0.1217
10	9.5046	-14.0796	-4.1453	21.3824	-7.8506	-11.8026	0.7109	1.3394	0.1033
1	9.1909	-12.4392	-4.6177	16.9708	-4.8493	-10.8744	0.7409	1.2230	0.1115
(e) S Maximum Likelihood									
100	11.5967	-21.5515	-1.2611	29.0403	-12.0714	-17.4030	0.6743	1.5201	0.1139
10	11.7491	-20.5710	-1.4935	23.7722	-8.5291	-16.5074	0.7117	1.4544	0.1083
1	10.7420	-16.8568	-3.2937	18.9453	-5.3403	-14.0510	0.7412	1.3206	0.1196
(f) R Maximum Likelihood									
100	4.0120	-3.3114	-6.6414	19.0588	-9.2450	-3.6237	0.6449	0.8590	0.1400
10	7.2131	-11.1833	-4.2032	20.6543	-8.4373	-9.5391	0.6966	1.3127	0.1167
1	5.3388	-6.4203	-6.1714	17.6832	-7.0595	-6.1650	0.7196	1.0634	0.1122

^aUnits of α_0 through β are \log_{10} (nT/min).

where magnetic activity is dominated by the equatorial electrojet, we do not use 1 min data from Huancayo, Peru (HUA, -1.13°N), since they cover a relatively short period of time (only since 1997). Therefore, Figure 4 is not especially accurate in a narrow band within a few latitude degrees of the geomagnetic equator, and we cannot resolve induction hazards there [e.g., Ngwira et al., 2013a; Carter et al., 2015].

At 55° geomagnetic latitude, corresponding to many large metropolitan areas of Northern Europe, Canada, and some in the United States, we estimate once-per-century ΔB_h , S , and R exceedances and 1σ ranges to be, respectively, 1000, [690, 1450]; 500, [350, 720]; and 200, [140, 280] nT/min. At 40° , corresponding to many large metropolitan areas of Southern Europe, the United States, and Australia, we estimate once-per-century ΔB_h , S , and R exceedances and 1σ values to be, respectively, 200, [140, 290]; 100, [70, 140]; and 40, [30, 60] nT/min.

8. Looking Forward

Numerical models of the coupled magnetosphere-ionosphere system [e.g., Weigel et al., 2003; Ngwira et al., 2013b; Pulkkinen et al., 2013] could be tested by comparing outputted dB/dt results with the latitude-dependent probability functions shown in Figure 4. With respect to induction hazards, recently, Bedrosian and Love [2015] showed that three-dimensional Earth conductivity results in substantial geographic differences in induced geoelectric fields—about 2 orders of magnitude difference across the midwestern United States. The convolution of reference geomagnetic activity functions similar to ΔB_h , S , and R through realistic Earth impedance functions and multiplied by the probability functions in Figure 4 would give an estimate of the probability that a geoelectric field of a certain size would be realized in a given geographic location. Such an exercise would inform the development of extreme-event geoelectric benchmarks needed to evaluate induction hazards [e.g., NSTC, 2015b, Goal 1.1].

Acknowledgments

We thank C. A. Finn, J. McCarthy, E. J. Rigler, and J. L. Slate for reviewing a draft manuscript. We thank P. A. Bedrosian, E. E. Bernabeu, J. Eichner, S. Jonas, A. Kelbert, and R. M. Waggel for useful conversations. The data were obtained from either the Kyoto or Edinburgh World Data Centers [e.g., Reay et al., 2013] or from INTERMAGNET [e.g., Love and Chulliat, 2013]. We thank the national institutes that support them and INTERMAGNET for promoting high standards of magnetic observatory practice (www.intermagnet.org). Part of this work was accomplished while J.J.L. was a visiting professor at the Université Paris Diderot in September 2015. This is IGP contribution 3729.

References

- Allen, J., L. Frank, H. Sauer, and P. Reiff (1989), Effects of the March 1989 solar activity, *Eos Trans. AGU*, 70(46), 1479–1488.
- Araki, T., et al. (1997), Anomalous sudden commencement on March 24, 1991, *J. Geophys. Res.*, 102, 14,075–14,086.
- Baker, D. N., et al. (2008), *Severe Space Weather Events—Understanding Societal and Economic Impacts*, Natl. Acad. Press, pp. 1–144, Washington, D. C.
- Balch, C., B. Murtagh, D. Zezula, L. Combs, G. Nelson, K. Tegnell, M. Crown, and B. McGehan (2004), *Service Assessment: Intense Space Weather Storms October 19–November 07, 2003*, US Dep. Commerce, NOAA, pp. 1–49, Silver Spring, Md.
- Bedrosian, P. A., and J. Love (2015), Mapping geoelectric fields during magnetic storms: Synthetic analysis of empirical United States impedances, *Geophys. Res. Lett.*, 42, 10,160–10,170, doi:10.1002/2015GL066636.
- Béland, J., and K. Small (2005), Space weather effects on power transmission systems: The cases of Hydro-Québec and Transpower New Zealand Ltd, in *Effects of Space Weather on Technology Infrastructure*, edited by I. A. Daglis, pp. 287–299, Springer, Dordrecht, Netherlands.
- Borovsky, J. E., R. J. Nemzek, and R. D. Belian (1993), The occurrence rate of magnetospheric-substorm onsets: Random and periodic substorms, *J. Geophys. Res.*, 98(A3), 3807–3813, doi:10.1029/92JA02556.
- Boteler, D. H. (2003), Geomagnetic hazards to conducting networks, *Nat. Hazards*, 28, 537–561.
- Cannon, P., et al. (2013), *Extreme Space Weather: Impacts on Engineered Systems and Infrastructure*, R. Acad. Eng., pp. 1–68, London, U. K.
- Carter, B. A., E. Yizengaw, R. Pradipta, A. J. Halford, R. Norman, and K. Zhang (2015), Interplanetary shocks and the resulting geomagnetically induced currents at the equator, *Geophys. Res. Lett.*, 42, 6554–6559, doi:10.1002/2015GL065060.
- Federal Energy Regulatory Commission (2013), Reliability standards for geomagnetic disturbances, *Fed. Regist. Rules Regul.*, 78(100), 30,747–30,762, Fed. Energy Reg. Comm.
- Hapgood, M. A. (2011), Towards a scientific understanding of the risk from extreme space weather, *Adv. Space Res.*, 47, 2059–2072.
- Kappenman, J. G. (2005), An overview of the impulsive geomagnetic field disturbances and power grid impacts associated with the violent Sun–Earth connection events of 29–31 October 2003 and a comparative evaluation with other contemporary storms, *Space Weather*, 3, S08C01, doi:10.1029/2004SW000128.
- Kappenman, J. G. (2006), Great geomagnetic storms and extreme impulsive geomagnetic field disturbance events—An analysis of observational evidence including the great storm of May 1921, *Adv. Space Res.*, 38, 188–199.
- Love, J. J. (2008), Magnetic monitoring of Earth and space, *Phys. Today*, 61(2), 31–37, doi:10.1063/1.2883907.
- Love, J. J., and A. Chulliat (2013), An international network of magnetic observatories, *Eos Trans. AGU*, 94(42), 373–374, doi:10.1002/2013EO420001.
- Love, J. J., E. J. Rigler, A. Pulkkinen, and C. C. Balch (2014), Magnetic storms and induction hazards, *Eos Trans. AGU*, 95(48), 445–446, doi:10.1002/2014EO480001.
- Love, J. J., E. J. Rigler, A. Pulkkinen, and P. Riley (2015), On the lognormality of historical magnetic storm intensity statistics: Implications for extreme-event probabilities, *Geophys. Res. Lett.*, 42, 6544–6553, doi:10.1002/2015GL064842.
- Milan, S. (2007), Auroral oval, in *Encyclopedia of Geomagnetism and Paleomagnetism*, edited by D. Gubbins and E. Herrero-Bervera, pp. 33–34, Springer, Dordrecht, Netherlands.
- North American Electric Reliability Corporation (NERC) (2014a), *Benchmark Geomagnetic Disturbance Event Description*, North Am. Electr. Reliab. Corp., pp. 1–26, Atlanta, Ga.
- NERC (2014b), *Transformer Thermal Impact Assessment: Project 2013-03 (Geomagnetic Disturbance Mitigation)*, North Am. Electr. Reliab. Corp., pp. 1–16, Atlanta, Ga.
- Ngwira, C. M., A. Pulkkinen, F. D. Wilder, and G. Crowley (2013a), Extended study of extreme geoelectric field event scenarios for geomagnetically induced current applications, *Space Weather*, 11, 121–131, doi:10.1002/swe.20021.
- Ngwira, C. M., A. Pulkkinen, M. Leila Mays, M. M. Kuznetsova, A. B. Galvin, K. Simunac, D. N. Baker, X. Li, Y. Zheng, and A. Gloer (2013b), Simulation of the 23 July 2012 extreme space weather event: What if the extremely rare CME was Earth-directed?, *Space Weather*, 11, 671–679, doi:10.1002/2013SW000990.
- National Science and Technology Council (NSTC) (2015a), *National Space Weather Strategy*, Executive Off., Natl. Sci. Technol. Council, pp. 1–13, Washington, D. C.
- NSTC (2015b), *National Space Weather Action Plan*, Executive Off., Natl. Sci. Technol. Council, pp. 1–38, Washington, D. C.
- Pirjola, R. (1984), Estimation of the electric field on the Earth's surface during a geomagnetic variation, *Geophysica*, 20, 89–103.
- Pulkkinen, A., S. Lindahl, A. Viljanen, and R. Pirjola (2005), Geomagnetic storm of 29–31 October 2003: Geomagnetically induced currents and their relation to problems in the Swedish high-voltage power transmission system, *Space Weather*, 3, S08C03, doi:10.1029/2004SW000123.
- Pulkkinen, A., R. Pirjola, and A. Viljanen (2008), Statistics of extreme geomagnetically induced current events, *Space Weather*, 6, S07001, doi:10.1029/2008SW000388.
- Pulkkinen, A., E. Bernabeu, J. Eichner, C. Beggan, and A. W. P. Thomson (2012), Generation of 100-year geomagnetically induced current scenarios, *Space Weather*, 10, S04003, doi:10.1029/2011SW000750.
- Pulkkinen, A., et al. (2013), Community-wide validation of geospace model ground magnetic field perturbation predictions to support model transition to operations, *Space Weather*, 11, 369–385, doi:10.1002/swe.20056.
- Reay, S. J., E. Clarke, E. Dawson, and S. Macmillan (2013), Operations of the World Data Centre for Geomagnetism, Edinburgh, *Data Sci. J.*, 12, WDS47–WDS51, doi:10.2481/dsj.WDS-005.
- Schrijver, C. J., et al. (2015), Understanding space weather to shield society: A global road map for 2015–2025 commissioned by COSPAR and ILWS, *Adv. Space Res.*, 55(12), 2745–2807, doi:10.1016/j.asr.2015.03.023.
- Thomson, A. W. P. (2007), Geomagnetic hazards, in *Encyclopedia of Geomagnetism and Paleomagnetism*, edited by D. Gubbins and E. Herrero-Bervera, pp. 316–319, Springer, Dordrecht, Netherlands.
- Thomson, A. W. P., A. J. McKay, E. Clarke, and S. J. Reay (2005), Surface electric fields and geomagnetically induced currents in the Scottish Power grid during the 30 October 2003 geomagnetic storm, *Space Weather*, 3, S11002, doi:10.1029/2005SW000156.
- Thomson, A. W. P., A. J. McKay, and A. Viljanen (2009), A review of progress in modelling of induced geoelectric and geomagnetic fields with special regard to induced currents, *Acta Geophys.*, 57, 209–219.
- Thomson, A. W. P., E. B. Dawson, and S. J. Reay (2011), Quantifying extreme behavior in geomagnetic activity, *Space Weather*, 9, S10001, doi:10.1029/2011SW000696.
- Trichtchenko, L., and D. H. Boteler (2007), Effects of recent geomagnetic storms on power systems, paper presented at 7th International Symposium on Electromagnetic Compatibility and Electromagnetic Ecology, pp. 265–268, Saint–Petersburg, 26–29 Jun., doi:10.1109/EMCECO.2007.4371706.

- Tsurutani, B. T., and G. S. Lakhina (2014), An extreme coronal mass ejection and consequences for the magnetosphere and Earth, *Geophys. Res. Lett.*, *41*, 287–292, doi:10.1002/2013GL058825.
- Viljanen, A. (1997), The relation between geomagnetic variations and their time derivatives and implications for estimation of induction risk, *Geophys. Res. Lett.*, *24*, 631–634.
- Viljanen, A., H. Nevanlinna, K. Pajunpää, and A. Pulkkinen (2001), Time derivative of the horizontal geomagnetic field as an activity indicator, *Ann. Geophys.*, *19*, 1107–1118.
- Weigel, R. S., A. J. Klimas, and D. Vassiliadis (2003), Solar wind coupling to and predictability of ground magnetic fields and their time derivatives, *J. Geophys. Res.*, *108*(A7), 1298, doi:10.1029/2002JA009627.